AMERICAN SOCIETY FOR MICROBIOLOGY

Infection and Immunity®

CCR2+ Inflammatory Monocytes Are Recruited to *Yersinia pseudotuberculosis* Pyogranulomas and Dictate Adaptive Responses at the Expense of Innate Immunity during Oral Infection

Yue Zhang,[a,b] Camille Khairallah,[a,b] Brian S. Sheridan,[a,b] Adrianus W. M. van der Velden,[a,b] James B. Bliska[a,b]

aCenter for Infectious Diseases, Stony Brook University, Stony Brook, New York, USA
bDepartment of Molecular Genetics and Microbiology, Stony Brook University, Stony Brook, New York, USA

ABSTRACT Murine Ly6C^{hi} inflammatory monocytes (IMs) require CCR2 to leave the bone marrow and enter mesenteric lymph nodes (MLNs) and other organs in response to *Yersinia pseudotuberculosis* infection. We are investigating how IMs, which can differentiate into CD11c$^+$ dendritic cells (DCs), contribute to innate and adaptive immunity to *Y. pseudotuberculosis*. Previously, we obtained evidence that IMs are important for a dominant CD8$^+$ T cell response to the epitope YopE$_{69-77}$ and host survival using intravenous infections with attenuated *Y. pseudotuberculosis*. Here we challenged CCR2$^{+/+}$ or CCR2$^{-/-}$ mice orally with wild-type *Y. pseudotuberculosis* to investigate how IMs contribute to immune responses during intestinal infection. Unexpectedly, CCR2$^{-/-}$ mice did not have reduced survival but retained body weight better and their MLNs cleared *Y. pseudotuberculosis* faster and with reduced lymphadenopathy compared to controls. Enhanced bacterial clearance in CCR2$^{-/-}$ mice correlated with reduced numbers of IMs in spleens and increased numbers of neutrophils in livers. *In situ* imaging of MLNs and spleens from CCR2-GFP mice showed that green fluorescent protein-positive (GFP$^+$) IMs accumulated at the periphery of neutrophil-rich *Yersinia*-containing pyogranulomas. GFP$^+$ IMs colocalized with CD11c$^+$ cells and YopE$_{69-77}$-specific CD8$^+$ T cells in MLNs, suggesting that IM-derived DCs prime adaptive responses in *Yersinia* pyogranulomas. Consistently, CCR2$^{-/-}$ mice had reduced numbers of splenic DCs, YopE$_{69-77}$-specific CD8$^+$ T cells, CD4$^+$ T cells, and B cells in organs and lower levels of serum antibodies to *Y. pseudotuberculosis* antigens. Our data suggest that IMs differentiate into DCs in MLN pyogranulomas and direct adaptive responses in T cells at the expense of innate immunity during oral *Y. pseudotuberculosis* infection.

KEYWORDS B lymphocytes, T lymphocytes, *Yersinia*, adaptive immunity, dendritic cells, granuloma, innate immunity, monocytes

Monocytes are an important subset of leukocytes that play critical and diverse roles in host immune responses to pathogen infection (1, 2). There are two murine monocyte types, characterized as Ly6C^{hi} or CX3CR1^{hi} cells. Ly6C^{hi} monocytes express CCR2 and low levels of CX3CR1. Ly6C^{hi} monocytes exit the bone marrow (BM) in a CCR2-dependent manner in response to inflammation and migrate to sites of infection. Ly6C^{hi} inflammatory monocytes can differentiate into macrophages or dendritic cells (DCs) and function by phagocytosis, secreting cytokines, transporting antigens, and priming T cells. CX3CR1^{hi} monocytes express low levels of Ly6C and CCR2. CX3CR1^{hi} monocytes patrol the luminal endothelium and can differentiate into macrophages in the intestinal lamina propria. Additionally, Ly6C^{hi} monocytes that are recruited to the

infected intestinal lamina propria can differentiate into CX3CR1^{int} inflammatory DCs (1, 2).

Diverse functions have been assigned to CCR2$^+$ Ly6C^{hi} inflammatory monocytes in bacterial infections (1, 2). During systemic *Listeria monocytogenes* infection, inflammatory monocytes can differentiate into Tip-DCs (tumor necrosis factor alpha [TNF-α]- and inducible nitric oxide synthase [iNOS]-producing DCs), which are critical for innate host protection (3). *In situ* imaging showed that IMs are recruited to foci of *L. monocytogenes* infection in spleen and liver (4). However, Tip-DCs were not required to induce CD8$^+$ or CD4$^+$ T cell responses in mice infected with *L. monocytogenes* (3). In a *Mycobacterium tuberculosis* aerosol infection model, IMs were not required to control initial bacterial growth in the lungs but were essential for priming a CD4$^+$ T cell response (5). In this capacity, the IMs transported *M. tuberculosis* from lung to lymph nodes, where DCs primed the CD4$^+$ T cell response (5). Therefore, during bacterial infection of mice, IMs can have distinct and important functions during innate and adaptive phases of immunity.

Yersinia pseudotuberculosis is an enteric Gram-negative zoonotic pathogen most commonly associated with mesenteric lymphadenitis in humans (6). Experimental intestinal infection of mice with *Y. pseudotuberculosis* results in bacterial colonization of Peyer's patches, the lamina propria, and mesenteric lymph nodes (MLNs) as well as dissemination to the spleen and liver (7, 8). Neutrophils and IMs are recruited to these organs in response to infection with *Y. pseudotuberculosis* (9–12). *Y. pseudotuberculosis* actively grows as extracellular microcolonies in these tissues (13), surrounded by recruited phagocytes (14). These organized clusters of immune cells surrounding *Y. pseudotuberculosis* were initially termed microabscesses (13) and more recently termed pyogranulomas (15), and the latter term is used here. The role of pyogranulomas in controlling immune responses to bacterial pathogens is unknown. *Y. pseudotuberculosis* uses a type III secretion system (T3SS) to inject phagocytes with Yop effectors (16, 17), thereby counteracting phagocytosis, the production of reactive oxygen species (ROS), and the release of cytokines (18). For example, the effector YopE, a GTPase-activating protein (GAP) for Rac1, Rac2, and RhoA, inhibits ROS production by phagocytes (19, 20). Because the T3SS effectors effectively disarm phagocytes (20–22), host control of *Y. pseudotuberculosis* infection requires additional components of innate immunity as well as adaptive responses. These include the NK cell component of innate immunity and CD8$^+$ T cell responses (23–25).

The delivery of T3SS effectors into phagocytes by *Y. pseudotuberculosis* provides antigen-presenting cells with a source of peptides that can be presented by major histocompatibility complex class I (MHCI) to CD8$^+$ T cells (26). *Y. pseudotuberculosis* YopE contains an immunodominant H-2K^b-restricted CD8$^+$ T cell epitope (YopE$_{69-77}$) located N terminal to the GAP domain (25, 27). Primary intestinal infection of C57BL/6 mice with wild-type *Y. pseudotuberculosis* results in a dominant CD8$^+$ T cell response to the YopE$_{69-77}$ epitope in intraepithelial lymphocytes, the lamina propria, MLN, spleen, and liver (11, 12, 25). Naive mice vaccinated with a YopE$_{69-77}$ peptide epitope are partially protected against subsequent lethal intestinal infection, indicating that pre-existing YopE$_{69-77}$-specific CD8$^+$ T cells can suffice for measurable immunity (25, 28, 29). YopE$_{69-77}$-specific CD8$^+$ T cells generated by vaccination or during primary *Y. pseudotuberculosis* infection produce the cytokines TNF-α and gamma interferon (IFN-γ), which likely mediate their protective effect (12, 29, 30).

We previously employed intravenous (i.v.) infection of mice with attenuated *Y. pseudotuberculosis* to investigate the features of YopE and the host immune response that are important for the production of large numbers of YopE$_{69-77}$-specific CD8$^+$ T cells (30, 31). An attenuated *yopE* GAP mutant was used for these studies because we found that YopE catalytic activity was not required for the large YopE$_{69-77}$-specific CD8$^+$ T cell response (30). Interestingly, CCR2$^{-/-}$ mice, which are defective for the recruitment of IMs out of bone marrow, had a significant defect in the production of YopE$_{69-77}$-specific CD8$^+$ T cells when they were infected with a *Y. pseudotuberculosis* *yopE* GAP mutant (31). Moreover, CCR2$^{-/-}$ mice were more susceptible to lethal

infection than wild-type controls, when they were infected with the *yopE* GAP mutant, suggesting that IMs are important for the control of *Y. pseudotuberculosis* in addition to their role in the production of YopE$_{69-77}$-specific CD8$^+$ T cells (31).

To extend the above-described results, here we investigated the role of IMs in immune responses during the natural oral route of infection with wild-type *Y. pseudotuberculosis*. Unexpectedly, we found that infected CCR2$^{-/-}$ mice were not more susceptible to lethality from oral infection but in fact retained body weight better starting at day 4 postinfection, rapidly cleared *Y. pseudotuberculosis* from MLNs, and had reduced mesenteric lymphadenopathy at day 14 postinfection compared to CCR2$^{+/+}$ controls. Thus, IMs appeared to contribute to *Y. pseudotuberculosis* persistence and lymphadenopathy in MLNs. *In situ* imaging of MLNs and spleens from CCR2-GFP mice showed that green fluorescent protein-positive (GFP$^+$) IMs were recruited to the periphery of neutrophil-rich *Yersinia*-containing pyogranulomas by as early as day 3 postinfection. The GFP$^+$ IMs colocalized with YopE$_{69-77}$-specific CD8$^+$ T cells, CD11c$^+$ cells, and Ly6G$^+$ neutrophils in MLNs, suggesting that IM-derived DCs prime adaptive responses in *Yersinia* pyogranulomas. Accordingly, CCR2$^{-/-}$ mice had reduced numbers of YopE$_{69-77}$-specific CD8$^+$ T cells, diminished numbers of CD4$^+$ T cells and B cells, and lower serum antibody responses to *Y. pseudotuberculosis* antigens at day 14 postinfection. Together, these data suggest that IMs recruited to *Yersinia* pyogranulomas contribute to lymphadenopathy and bacterial persistence in MLNs while at the same time promoting adaptive immune responses during oral infection. CCR2$^{-/-}$ mice with reduced adaptive immunity may be protected from lethality from oral *Y. pseudotuberculosis* infection in part by compensating with decreased mesenteric lymphadenopathy and increased innate responses in the absence of IMs.

RESULTS

Role of CCR2 in host survival, bacterial colonization, and mesenteric lymphadenopathy during oral *Yersinia* infection. We previously showed that CCR2 is required for host survival and a dominant CD8$^+$ T cell response to the YopE$_{69-77}$ epitope when mice are infected i.v. with a *yopE* GAP mutant strain of *Y. pseudotuberculosis* (31). To further investigate the role of CCR2 as well as the IMs whose egress from BM requires this receptor (1, 2), we established an oral infection model using wild-type *Y. pseudotuberculosis* strain 32777. To mimic the natural route of oral infection, a bread-feeding procedure used previously for *L. monocytogenes* was employed (32). Unexpectedly, at three different infectious doses, the percentages of C57BL/6 (CCR2$^{+/+}$) and CCR2$^{-/-}$ mice that survived infection were similar (Fig. 1A to C). In addition, of the mice that survived challenge with middle or low doses of *Y. pseudotuberculosis*, CCR2$^{-/-}$ mice lost less than 5% of their body weight on average (Fig. 1D). C57BL/6 mice lost ~10% of their body weight on average before they recovered, and the difference in body weights between the two groups became significant starting at 4 days postinfection (dpi) (Fig. 1D). These results suggested the possibility that in CCR2$^{-/-}$ mice, the immune response is altered in favor of the host compared to C57BL/6 mice, although the survival outcomes are similar.

To further analyze the course of infection and immune response, additional groups of C57BL/6 and CCR2$^{-/-}$ mice were infected at 5×10^7 CFU, and bacterial burdens (CFU) in the MLN, spleen, and liver were determined at 3, 7, and 14 dpi. In MLNs, similar colonization levels were maintained from days 3 to 7 postinfection for both groups of mice (Fig. 1E). Most of the CCR2$^{-/-}$ mice cleared the bacteria from MLNs by 14 dpi; however, the majority of the C57BL/6 mice still carried bacteria at this time, and the difference between the two groups was significant ($P = 0.0038$) (Fig. 1E). Bacterial colonization in spleen and liver followed similar patterns in C57BL/6 and CCR2$^{-/-}$ mice from days 3 to 7 postinfection, as CFU levels increased equally in both groups (Fig. 1F and G). By day 14, the colonization levels decreased in both organs in both groups of mice, although at this time point, the majority of CCR2$^{-/-}$ mice had no CFU in spleen, while most C57BL/6 mice still had bacteria in this organ, although this difference was
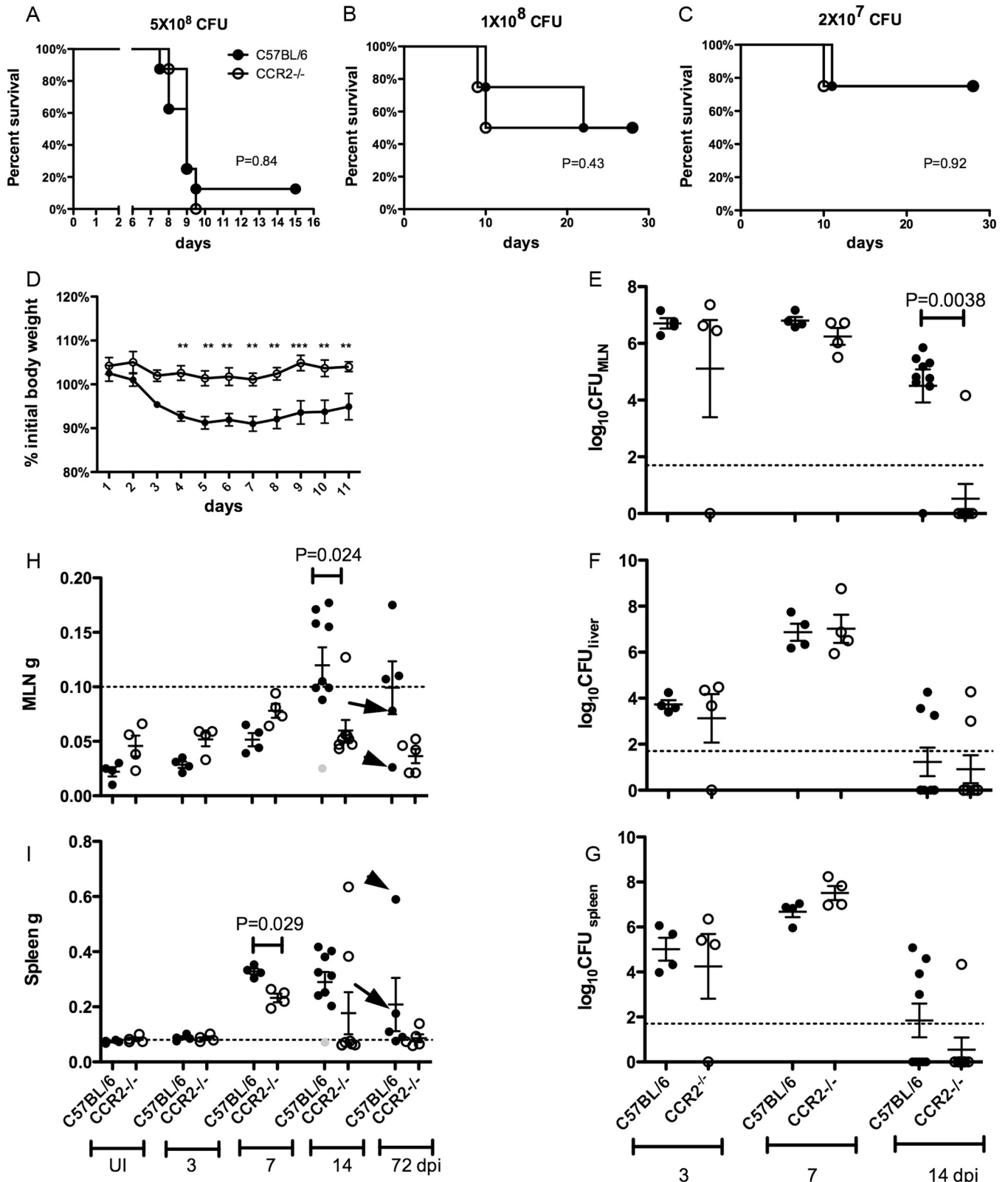
FIG 1 Similar host survival rates but reduced weight loss, bacterial colonization, and mesenteric lymphadenitis in the absence of CCR2. (A to C) Survival of C57BL/6 or CCR2$^{-/-}$ mice after oral infection with *Y. pseudotuberculosis* 32777 at 5×10^8 CFU (A), 1×10^8 CFU (B), or 2×10^7 CFU (C). The *P* values were determined by a log rank test, and the numbers of mice used were 8 (A) or 4 (B and C) of each genotype. (D) Percentage of initial body weight of the surviving mice analyzed in panels B and C to 11 dpi. Means and standard errors are shown, ** indicates *P* values of <0.01, and *** indicates *P* values of <0.001, as calculated with two-way repeated-measures analysis of variance (ANOVA) followed by a Bonferroni posttest. (E to G) C57BL/6 or CCR2$^{-/-}$ mice were orally infected with 5×10^7 CFU of 32777, and bacterial colonization levels in MLN (E), liver (F), and spleen (G) were determined by CFU assays at 3, 7, and 14 dpi.

(Continued on next page)

not significant ($P = 0.23$) (Fig. 1G). Thus, CCR2$^{-/-}$ mice appeared to eliminate the bacteria from lymphoid organs, but not liver, more efficiently than did C57BL/6 mice.

Chronic mesenteric lymphadenopathy was previously shown to be triggered by oral *Y. pseudotuberculosis* infection of C57BL/6 mice (12). To investigate the role of CCR2 in this process, the weights of MLNs in the two groups of mice were also determined before and during infection. The average weight of the MLNs of naive CCR2$^{-/-}$ mice was higher than that of the MLNs of C57BL/6 mice, although the difference was not significant ($P = 0.15$) (Fig. 1H). From days 3 to 7 postinfection, the average weights of MLNs of both groups of mice increased, with the average weight of CCR2$^{-/-}$ MLNs being slightly higher, but the difference was not significant ($P = 0.057$) (Fig. 1H). At 14 dpi, the average weight of CCR2$^{-/-}$ MLNs decreased from the peak levels observed at 7 dpi (Fig. 1H). In contrast, the average weight of MLNs of C57BL/6 mice more than doubled from days 7 to 14 postinfection and was significantly higher than that of MLNs of CCR2$^{-/-}$ mice ($P = 0.024$) (Fig. 1H). The weights of MLNs were additionally determined at 72 dpi in C57BL/6 and CCR2$^{-/-}$ mice that survived the experiments shown in Fig. 1B and C. Three of five of the C57BL/6 MLNs were heavier than the 100-mg threshold for lymphadenopathy (12), while the weights of all CCR2$^{-/-}$ MLNs were similar to those of MLNs of uninfected mice, although the difference between the two groups at this time was not significant ($P = 0.057$) (Fig. 1H). Changes in spleen weights of the two groups of mice followed a similar pattern of temporal enlargement that peaked at around 7 dpi, although the average weight of infected spleens from C57BL/6 mice was significantly higher ($P = 0.029$) at this time point (Fig. 1I). After this time, the average spleen weights of both groups decreased, although that of infected CCR2$^{-/-}$ mice decreased faster (Fig. 1I). The three mice with enlarged MLNs at 72 dpi did not have enlarged spleens (Fig. 1H and I), indicating that chronic lymphadenopathy was unique to MLNs. Of note, the two CCR2$^{-/-}$ mice with enlarged spleens at 14 dpi were found in subsequent analyses to have adaptive immune responses that were distinct from those of the rest of the CCR2$^{-/-}$ mice but resembled those of wild-type mice, and in the following descriptions, these two mice were omitted from the CCR2$^{-/-}$ group. Overall, these results suggest that CCR2$^{-/-}$ mice have reduced persistence of *Y. pseudotuberculosis* and lymphadenopathy in MLNs.

Diminished recruitment of IMs to peripheral tissues in the absence of CCR2. To confirm that the egress of Ly6C^{hi} IMs from BM and entry into tissues were dependent on CCR2 during oral *Y. pseudotuberculosis* infection, we quantified these cells in both naive and infected C57BL/6 and CCR2$^{-/-}$ mice by flow cytometry. In naive C57BL/6 mice, the largest numbers of Ly6C^{hi} CD11b$^+$ IMs were found in BM and spleens (Fig. 2A to C). The other peripheral tissues analyzed, blood, liver, or MLN, contained 10- to 100-fold fewer IMs than did BM (see Fig. S1 in the supplemental material). CCR2$^{-/-}$ mice had numbers of IMs in BM similar to those found in C57BL/6 mice, and fewer such cells in all peripheral tissues, as expected (Fig. 2A to C and Fig. S1). Infection with *Y. pseudotuberculosis* resulted in the rapid induction and recruitment of IMs to blood and organs analyzed in C57BL/6 mice, especially from days 3 to 7 postinfection, with a peak at around 7 dpi (Fig. 2A to C and Fig. S1). As expected, infected CCR2$^{-/-}$ mice harbored many fewer IMs in all peripheral tissues analyzed during the course of infection, and the difference in the spleens at 7 dpi was significant compared to C57BL/6 mice (Fig. 2C). At 14 dpi, consistent with the decreased overall bacterial burdens compared to those at 7 dpi, the numbers of IMs in both C57BL/6 and CCR2$^{-/-}$ mice decreased dramatically

FIG 1 Legend (Continued)
The dotted line indicates the detection limit, and the means and standard errors are indicated. (H and I) Weights of MLNs (H) or spleens (I) from uninfected (UI) mice or mice infected for the indicated numbers of days postinfection, with means and standard errors indicated. The infection dose for 3, 7, and 14 dpi was 5×10^7 CFU, and that for 72 dpi was 1×10^8 or 2×10^7 CFU. Gray symbols at 14 dpi indicate a C57BL/6 mouse that had no detectable *Y. pseudotuberculosis* bacteria in all the tissues analyzed. At 72 dpi, one C57BL/6 mouse was highly colonized ($>1 \times 10^6$ CFU) in the MLN (arrows), and another was highly colonized in the liver (arrowheads). For panels E to I, each spot represents the value obtained from one mouse. Data shown are combined from two to three experiments (A and E to I) or from a single experiment (B and C). In panel H, the dotted line indicates the 100-mg cutoff for chronic lymphadenopathy, and in panel I, the dotted line indicates the average weight of uninfected spleens. For panels E to I, P values were calculated with the Mann-Whitney, test and P values of <0.05 are indicated.
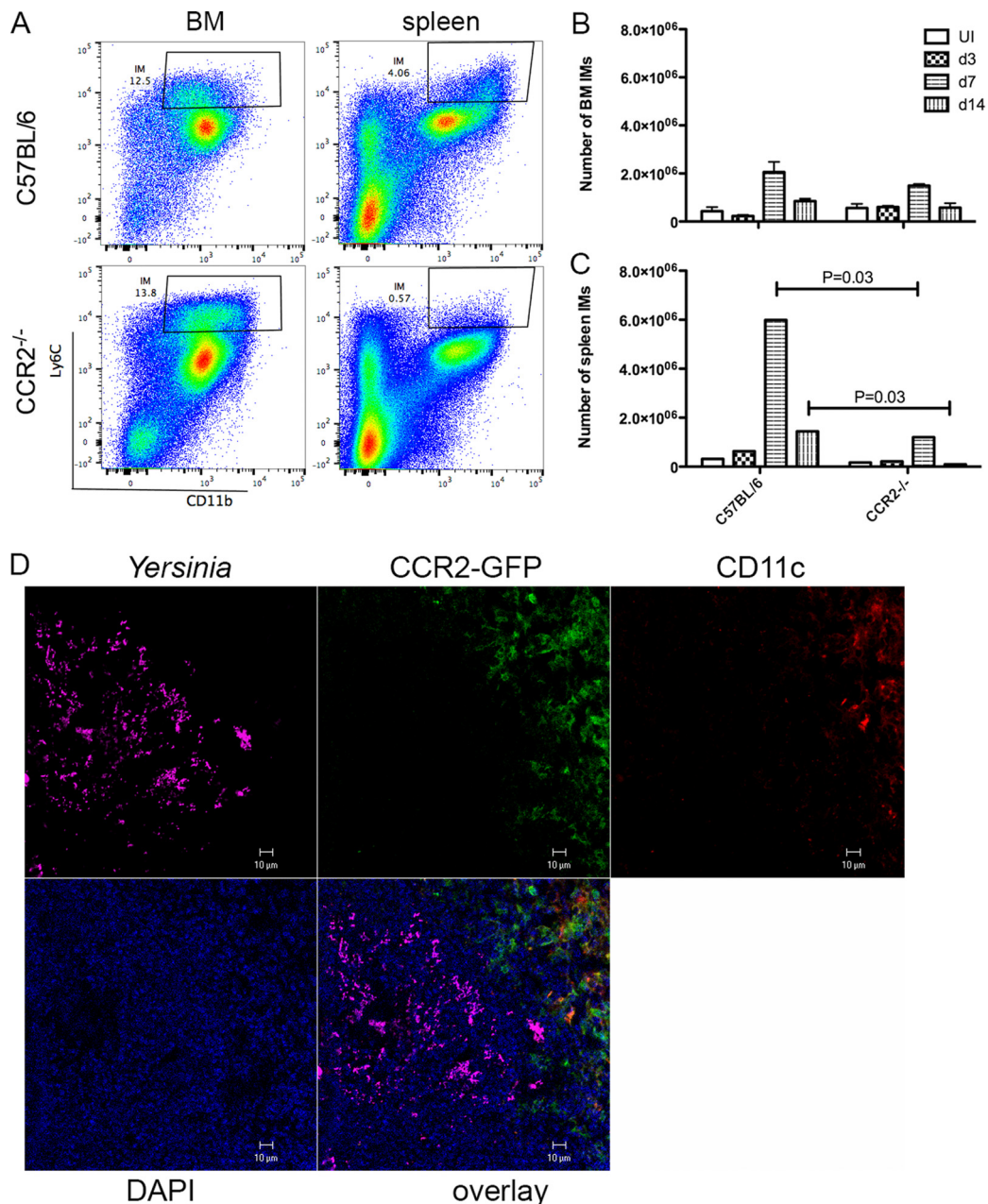
FIG 2 CCR2-dependent recruitment of IMs to peripheral tissues and localization of these cells to *Yersinia* infection foci. C57BL/6, CCR2$^{-/-}$, or CCR2-GFP mice were orally infected with 5×10^7 CFU of 32777. (A to C) Cells were isolated from bone marrow (BM) or spleen at 7 or 14 dpi, stained with anti-Ly6G and anti-CD11b, and analyzed by flow cytometry. Dead cells were excluded from the analysis. (A) Representative dot plots of Ly6C and CD11b signals of cells isolated from either BM or spleen of C57BL/6 (top) or CCR2$^{-/-}$ (bottom) mice at 7 dpi. The gate indicates CD11b$^+$ Ly6C^{hi} IMs. (B and C) The numbers of IMs from BM (B) or spleen (C) in mice left uninfected (UI) or at the indicated number of days postinfection calculated from the flow cytometry data are plotted. Data shown are the means and standard errors of data from individual animals combined from at least two independent experiments. *P* values were calculated with a Mann-Whitney test, and *P* values of <0.05 are indicated. (D) Tissues from CCR2-EGFP mice after infection were fixed, and frozen sections were prepared and stained with DAPI, anti-*Yersinia* polyclonal antibody, and anti-CD11c antibody followed by fluorescently labeled species-specific secondary antibodies for confocal microscopy. Representative confocal immunofluorescence microscopic images of individual and overlaid fluorescent signals, as indicated, from one spleen at 3 dpi are shown.

in all tissues analyzed, but the numbers of IMs in CCR2$^{-/-}$ mice were much lower, and the differences in the numbers of IMs from all peripheral tissues were significant between the two groups (Fig. 2C and Fig. S1). This result confirmed a defect of IM recruitment to the peripheral tissues of *Yersinia*-infected CCR2$^{-/-}$ mice.

IMs are recruited to the outskirts of *Yersinia* infection foci. To visualize the location of recruited IMs, we carried out *in situ* imaging of spleen sections from CCR2-GFP mice (33) orally infected with *Y. pseudotuberculosis*. We identified IMs as GFP$^+$ cells and used antibody staining to detect *Y. pseudotuberculosis* and CD11c$^+$ DCs. At 3 dpi, the majority of *Y. pseudotuberculosis* signals were found in confined areas, some clustered together in a microcolony, more distributed around cells (Fig. 2D, purple). Curiously, GFP$^+$ cells were concentrated adjacent to the areas rich in *Y. pseudotuberculosis* bacteria. There were GFP$^+$ cells very close to *Y. pseudotuberculosis* bacteria, but the most prominent feature is that the area of the GFP signal was juxtaposed with the *Y. pseudotuberculosis*-rich area, and the GFP signals intermingled with the CD11c signals (Fig. 2D, red), which is consistent with our previously reported data showing that IMs differentiate into CD11c$^+$ inflammatory DCs (31). Overall, these results indicate that by as early as 3 dpi, IMs are recruited to and concentrated at the outskirts of *Yersinia* infection foci.

Recruitment of neutrophils to peripheral tissues in the absence of CCR2. There is an influx of neutrophils as well as IMs from BM into the MLN, spleen, and liver of C57BL/6 mice orally infected with *Y. pseudotuberculosis* (9, 10, 12). To determine if CCR2 deficiency affects neutrophil recruitment, the numbers of CD19$^-$ CD3$^-$ CD11b$^+$ Ly6G$^+$ cells in various tissues of C57BL/6 and CCR2$^{-/-}$ mice before and after oral infection with *Y. pseudotuberculosis* were measured by using flow cytometry (Fig. 3A). Unexpectedly, in naive mice, more neutrophils were identified in BM and MLNs of CCR2$^{-/-}$ mice ($P = 0.02$ and 0.04, respectively) (Fig. 3B and D). The trend of more neutrophils in peripheral organs of CCR2$^{-/-}$ mice continued after infection. In most organs analyzed at 3 dpi and all tissues analyzed at 7 dpi, more neutrophils were identified in CCR2$^{-/-}$ mice, and the difference was significant in liver at 7 dpi (Fig. 3C to E). This trend reversed, however, with the clearance of *Y. pseudotuberculosis* bacteria in CCR2$^{-/-}$ mice at 14 dpi. The numbers of neutrophils decreased dramatically, and, with the exception of BM, higher numbers of neutrophils were observed in C57BL/6 mice for all the organs examined (Fig. 3C to E). Thus, before infection and up to 7 dpi, there was a trend toward or significantly more neutrophils in tissues of CCR2$^{-/-}$ mice than in C57BL/6 mice. On the other hand, the large increase in the number of neutrophils in C57BL/6 MLNs between days 7 and 14 postinfection (Fig. 3D) likely contributed to the increased lymphadenopathy compared to that of CCR2$^{-/-}$ MLNs at this time point (Fig. 1H).

Recruitment of neutrophils to the center of *Yersinia* infection foci to form pyogranulomas with IMs. The relative location of neutrophils, IMs, and *Y. pseudotuberculosis* bacteria was determined by *in situ* imaging of MLNs of CCR2-GFP mice at 3 and 6 dpi (Fig. 3F and G). At 3 dpi, an area of dispersed *Y. pseudotuberculosis* signals was intermingled and fully encapsulated with Ly6G$^+$ neutrophils (Fig. 3F). Toward the outskirts of the *Y. pseudotuberculosis*-neutrophil region, the signal strength of Ly6G decreased, and the GFP$^+$ IM signal gradually increased, although some GFP$^+$ cells penetrated deep into the lesion formed in the area of *Y. pseudotuberculosis* localization (Fig. 3F). With the progression of infection at 6 dpi, there was a contraction of the immune cell and *Yersinia* signals, but the spatial arrangement of a ring of IMs surrounding neutrophils, which enclosed *Y. pseudotuberculosis* bacteria in a pyogranuloma, was maintained (Fig. 3G). The spatial location of leukocytes within the pyogranulomas suggested a direct role for neutrophils in controlling *Y. pseudotuberculosis* infection and a facilitating and/or regulatory role for IMs in the immune response.

CCR2 is required for a large YopE$_{69-77}$-specific CD8$^+$ T cell response. Next, the adaptive immune response was analyzed. To determine if CCR2 is required for a robust antigen-specific CD8$^+$ T cell response during oral *Y. pseudotuberculosis* infection, cells from various tissues of C57BL/6 or CCR2$^{-/-}$ mice were analyzed by flow cytometry after staining with the YopE$_{69-77}$ tetramer. In C57BL/6 mice, 6 days after oral infection with *Y. pseudotuberculosis* is the earliest time when YopE$_{69-77}$-specific CD8$^+$ T cells can be detected at levels significantly above the levels in naive mice, and their levels in circulation peak at around 9 dpi (data not shown) (11). Figure 4A shows representative
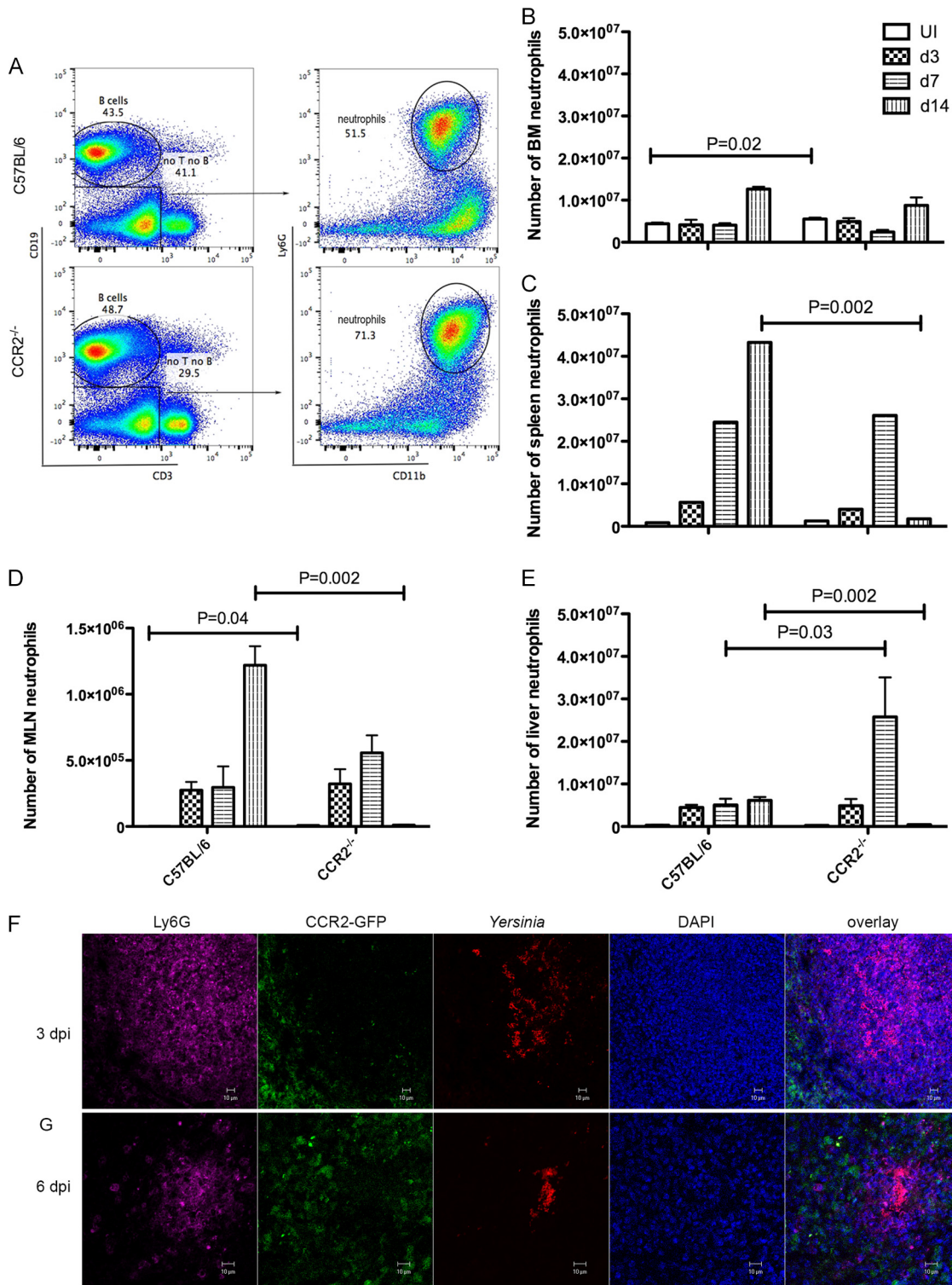
FIG 3 Recruitment of neutrophils to peripheral tissues in the absence of CCR2 and localization of these cells in pyogranulomas with IMs. Mice were left uninfected (UI) or infected, and tissues were collected and processed as described in the legend to Fig. 2. (A to E) Cells from the indicated tissues were analyzed by flow cytometry. (A) Representative dot plots of CD19-CD3 (left) signals of viable splenocytes and Ly6G-CD11b (right) signals of gated CD19⁻ CD3⁻ cells of C57BL/6 (top) or CCR2⁻/⁻ (bottom) mice at 7 dpi. (B to E) The numbers of neutrophils from BM (B), spleen (C), MLN (D), and liver (E) of uninfected mice or mice at the indicated days postinfection were determined and are plotted. Means and standard errors shown are the summaries of data from two or more independent experiments. Significant differences between C57BL/6 and CCR2⁻/⁻ mice were calculated with a Mann-Whitney test, P values of <0.05 are indicated. In panel D, the numbers of polymorphonuclear leukocytes in MLNs of uninfected C57BL/6 and CCR2⁻/⁻ mice were 2,166 ± 410 and 7,943 ± 1,755, respectively. (F and G) Representative confocal microscopic images of individual and overlaid immunofluorescent signals, as indicated, from frozen sections of MLNs of CCR2-GFP mice infected with 32777 at 3 dpi (F) and 6 dpi (G).
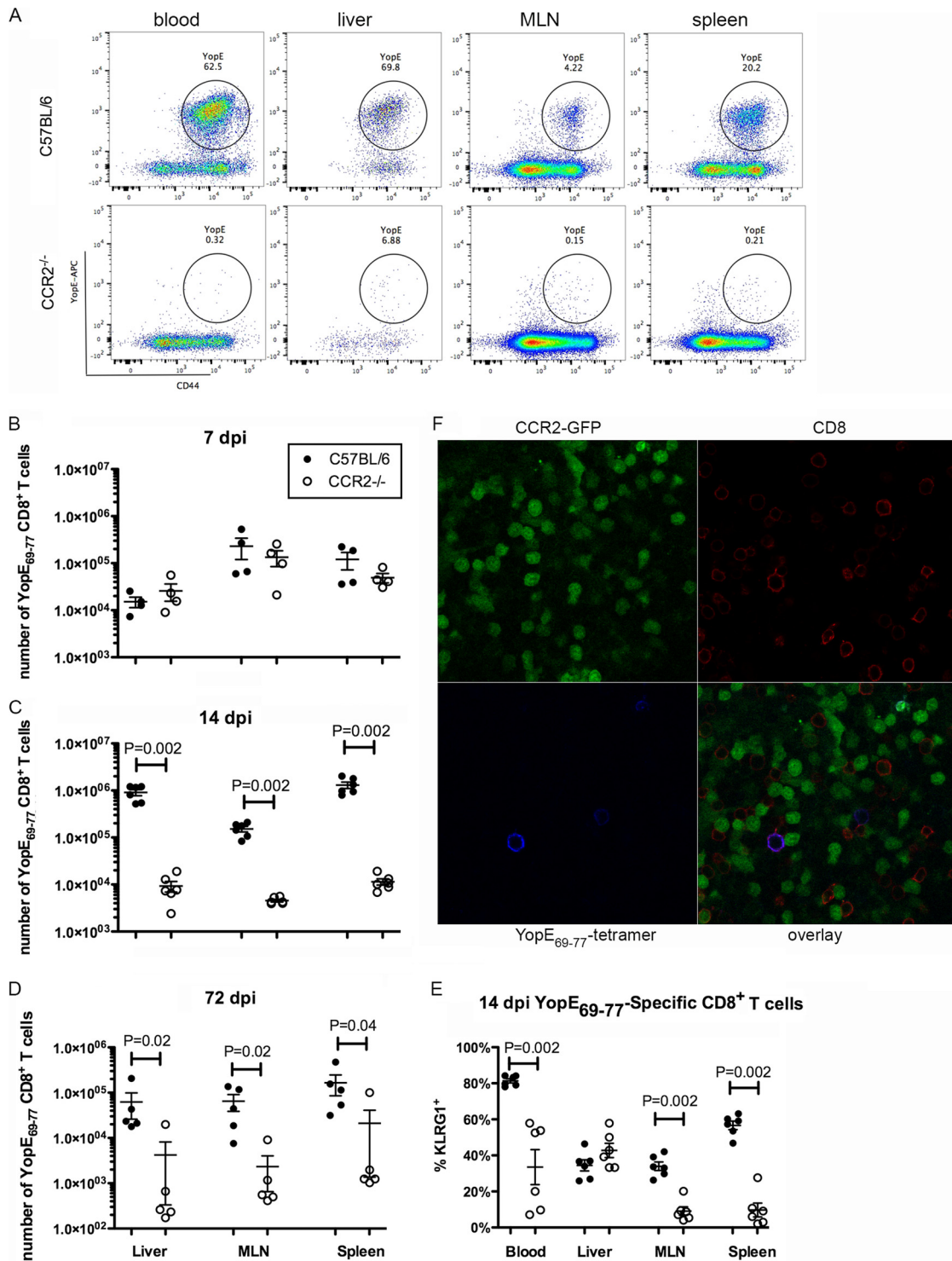
FIG 4 CCR2 is required for formation of large numbers of YopE$_{69-77}$-specific CD8 T cells. Mice were infected orally with 5×10^7 CFU of 32777, as described in the legend to Fig. 2. (A to E) Cells from the indicated tissues were subjected to flow cytometry following staining with the tetramer and a panel of antibodies. (A) Representative dot plots of YopE$_{69-77}$ tetramer and CD44 signals of gated CD45.2$^+$ CD3$^+$ CD8$^+$ T cells from the indicated tissues at 14 dpi. (B to D) Numbers of YopE$_{69-77}$-specific CD8$^+$ T cells at 7 dpi (B), 14 dpi (C), or 72 dpi (D) are plotted. The numbers of YopE$_{69-77}$-specific CD8$^+$ T cells in uninfected C57BL/6 and CCR2$^{-/-}$ mice were $0.73 \times 10^4 \pm 0.43 \times 10^4$ and $1.6 \times 10^4 \pm 0.60 \times 10^4$ (liver), $0.37 \times 10^4 \pm 0.27 \times 10^4$ and $0.33 \times 10^4 \pm 0.18 \times 10^4$ (MLN), and $0.81 \times 10^4 \pm 0.30 \times 10^4$ and $1.74 \times 10^4 \pm 0.98 \times 10^4$ (spleen), respectively. (E) Percentages of tetramer-positive CD8$^+$ cells that are also positive for the effector marker KLRG1 at 14 dpi. Data shown are the summaries of results from two or more independent experiments, with means and standard errors indicated. *P* values were determined with the Mann-Whitney test, and *P* values of <0.05 are indicated. (F) Fresh thick sections of MLN were prepared from an infected CCR2-GFP mouse at 7 dpi and stained with the YopE$_{69-77}$ tetramer conjugated with APC and CD8α antibodies as described in Materials and Methods. Representative confocal microscopy images of indicated individual and overlaid fluorescent signals are shown.

dot plots of gated $CD8^+$ T cells at 14 dpi stained additionally with the $YopE_{69-77}$ tetramer and anti-CD44 (a marker of activation). Cumulative results at 7, 14, and 72 dpi are shown in Fig. 4B to D. Values from control uninfected mice are reported in the legend to Fig. 4. At 7 dpi, there were similar numbers of $YopE_{69-77}$-specific $CD8^+$ T cells in the liver, MLN, and spleen between C57BL/6 and $CCR2^{-/-}$ mice (Fig. 4B). The number of $YopE_{69-77}$-specific $CD8^+$ T cells in C57BL/6 mice increased 10- to 100-fold between 7 and 14 dpi, mostly in livers and spleens (Fig. 4B and C). In contrast, in infected $CCR2^{-/-}$ mice, the average number of $YopE_{69-77}$-specific $CD8^+$ T cells decreased slightly in all the tissues analyzed from days 7 to 14 postinfection, and the decrease in MLNs was most dramatic (Fig. 4B and C). As a result, at 14 dpi, there were significantly fewer $YopE_{69-77}$-specific $CD8^+$ T cells in these tissues in $CCR2^{-/-}$ mice than in C57BL/6 mice (Fig. 4C). Not only was the average number of antigen-specific $CD8^+$ T cells lower in multiple tissues in infected $CCR2^{-/-}$ mice at 14 dpi, a lower percentage of these cells bore the effector marker KLRG1, and the differences in blood, MLN, and spleen were statistically significant (Fig. 4E). Thus, consistent with data from our previously reported i.v. infection model, oral challenge with *Y. pseudotuberculosis* resulted in the stimulation of $YopE_{69-77}$-specific effector $CD8^+$ T cells, and this process required $CCR2^+$ IMs. The highest numbers of $YopE_{69-77}$-specific effector $CD8^+$ T cells were found in livers and spleens (Fig. 4C), which also contained the highest numbers of IMs, indicating a correlation in the tissue distributions of these two cell types. Additionally, at 72 dpi, there were significantly fewer $YopE_{69-77}$-specific $CD8^+$ T cells in livers, MLNs, and spleens of $CCR2^{-/-}$ mice than in C57BL/6 mice (Fig. 4D), suggesting that $CCR2^+$ IMs are important for a memory response.

Flow cytometry was used to quantify $MHCII^+$ $CD11c^+$ cells, which would include IM-derived DCs (31) and conventional DCs, in spleens of uninfected and infected C57BL/6 and $CCR2^{-/-}$ mice at 3, 7, and 14 dpi. As shown in Fig. S3 in the supplemental material, the numbers of $MHCII^+$ $CD11c^+$ cells significantly increased in C57BL/6 spleens at between 3 and 7 dpi and remained elevated at 14 dpi, but this increase did not occur in $CCR2^{-/-}$ spleens. At 14 dpi, there were significantly fewer $MHCII^+$ $CD11c^+$ cells in $CCR2^{-/-}$ spleens than in C57BL/6 spleens (Fig. S3A and S3B). The reduced numbers of $MHCII^+$ $CD11c^+$ cells in $CCR2^{-/-}$ spleens at 14 dpi was likely due to the absence of IMs that could serve to replenish the pool of DCs and was correlated with the inability of $YopE_{69-77}$-specific $CD8^+$ T cells to expand at between 7 and 14 dpi (Fig. 4B and C) in these mice.

$YopE_{69-77}$-specific $CD8^+$ T cells colocalize with IMs, neutrophils, and DCs in pyogranulomas. *In situ* tetramer staining (34) was used to determine the location of $YopE_{69-77}$-specific $CD8^+$ T cells and GFP^+ IMs in the MLNs of CCR2-GFP mice at 6 dpi. $YopE_{69-77}$-specific $CD8^+$ T cells were found in the regions enriched in GFP^+ IMs (Fig. 4E). Additional *in situ* tetramer staining of MLNs at 6 or 7 dpi was done to visualize GFP^+ IMs, $Ly6G^+$ neutrophils, and $CD11c^+$ DCs (see Fig. S2 in the supplemental material). In addition to contacting IMs, $YopE_{69-77}$-specific $CD8^+$ T cells were intermingled with or very close to either $Ly6G^+$ neutrophils (Fig. S2A) or $CD11c^+$ DCs (Fig. S2B). We were not able to detect *Y. pseudotuberculosis* in these samples due to the requirement for the use of unfixed samples in the first step of *in situ* tetramer staining. Nevertheless, these results are consistent with the idea (31) that IMs in contact with *Y. pseudotuberculosis* and injected with YopE differentiate into $CD11c^+$ inflammatory DCs and directly prime $YopE_{69-77}$-specific $CD8^+$ T cells in pyogranulomas.

Reduced $CD4^+$ T cell and B cell numbers and serum antibody responses in the absence of CCR2. We next set out to determine if other aspects of adaptive immunity are impaired in *Y. pseudotuberculosis*-infected $CCR2^{-/-}$ mice. We first measured numbers of B cells in livers, MLNs, and spleens from C57BL/6 and $CCR2^{-/-}$ mice left uninfected or infected for 7 or 14 days. $CD19^+$ $CD3^-$ B cells were quantified by flow cytometry (Fig. 3A). B cell numbers in the tissues did not substantially increase in response to infection, but at both 7 and 14 dpi, C57BL/6 mice harbored significantly more B cells in their spleens than did $CCR2^{-/-}$ mice (Fig. 5A and B). Additionally, MLNs of infected C57BL/6 mice contained more B cells than did MLNs of infected $CCR2^{-/-}$
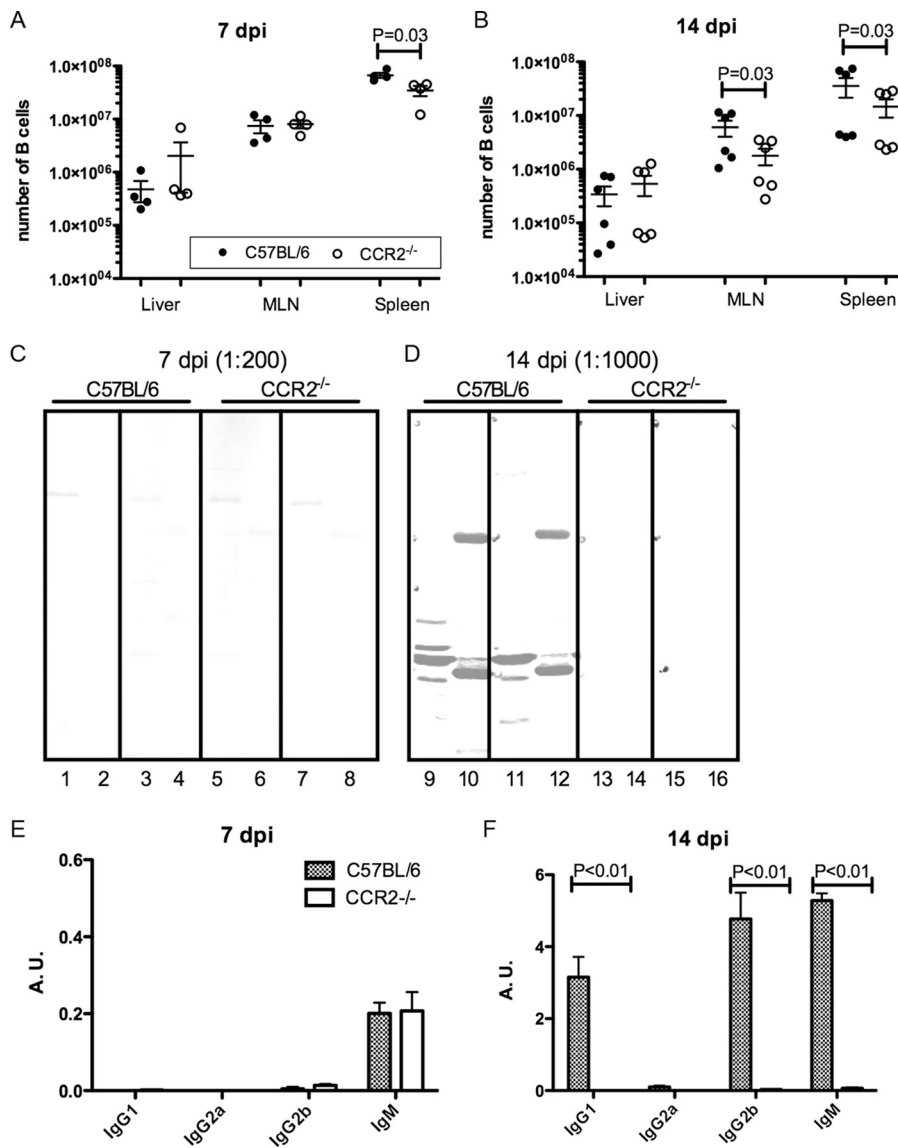
FIG 5 Reduced B cell numbers and diminished serum antibody responses in the absence of CCR2. C57BL/6 or CCR2$^{-/-}$ mice were infected orally with 5×10^7 CFU of 32777. (A and B) The numbers of CD19$^+$ CD3$^-$ B cells in the indicated tissues at 7 dpi (A) or 14 dpi (B) were determined by flow cytometry as described in the legend to Fig. 3A, with means and standard errors indicated. *P* values were determined with a Mann-Whitney test, and *P* values of <0.05 are indicated. The numbers of B cells in uninfected C57BL/6 and CCR2$^{-/-}$ mice were $1.19 \times 10^6 \pm 0.48 \times 10^6$ and $1.15 \times 10^6 \pm 0.53 \times 10^6$ (liver), $1.66 \times 10^6 \pm 0.23 \times 10^6$ and $4.42 \times 10^6 \pm 1.13 \times 10^6$ (MLN), and $25.43 \times 10^6 \pm 3.27 \times 10^6$ and $37.06 \times 10^6 \pm 4.02 \times 10^6$ (spleen), respectively. (C and D) Representative quantitative immunoblot analysis of the bacterial lysate (odd-numbered lanes) and secreted Yops (even-numbered lanes) using sera collected from mice of the indicated genotypes at 7 dpi (C) or 14 dpi (D). Each strip represents the signal obtained from one serum sample. (E and F) The recognition of secreted Yops by different subclasses of antibodies was determined by an ELISA with serum collected at 7 dpi (E) or 14 dpi (F). Means absorbance units (A.U.) and standard errors shown are the summaries of results from sera collected from at least two experiments at each time point. *P* values were determined with two-way ANOVA and Bonferroni posttests, and *P* values of <0.05 are indicated.

mice at 14 dpi (Fig. 5B). This pointed to a potential defect in the antibody response in CCR2$^{-/-}$ mice.

Serum from individual mice was used for immunoblotting to detect the antibody recognition of *Y. pseudotuberculosis* antigens in whole bacterial lysates or secreted Yops (Fig. 5C and D). At 7 dpi, a weak serum antibody response was detected from infected C57BL/6 mice (Fig. 5C), and the signal strength increased greatly at 14 dpi (Fig. 5D). In contrast, even though a similarly weak antibody response was detected at 7 dpi in the
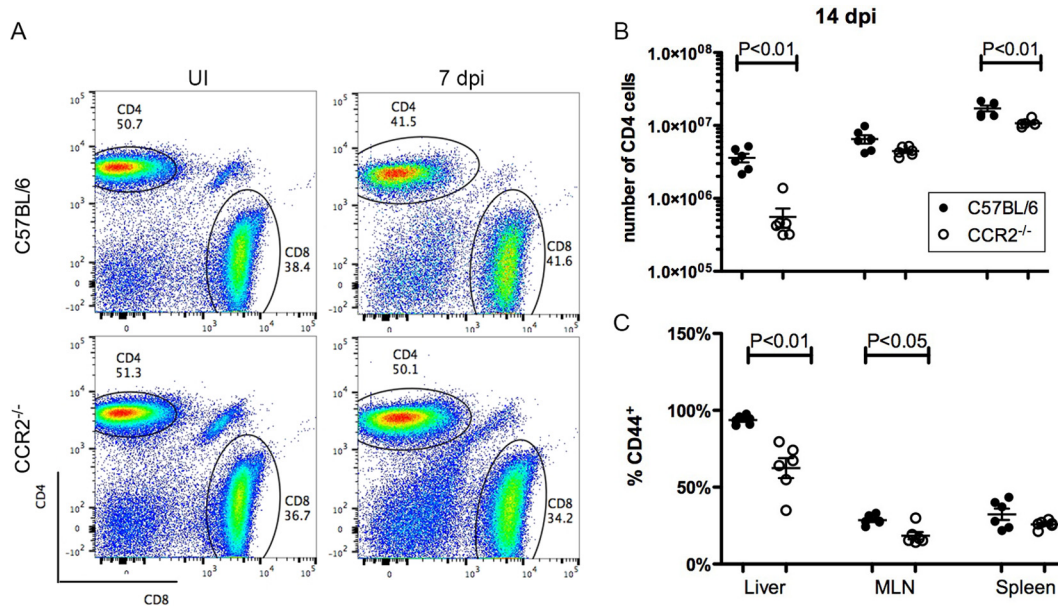
FIG 6 Decreased CD4$^+$ T cell response in the absence of CCR2. C57BL/6 or CCR2$^{-/-}$ mice were infected orally with 5 $\times$ 10^7 CFU of 32777. (A) Representative dot plots of gated CD45.2$^+$ CD3$^+$ cells from the spleens of uninfected (UI) mice (left) or infected C57BL/6 (top) or CCR2$^{-/-}$ (bottom) mice at 7 dpi (right) depicting the signals of CD8 and CD4. (B) Numbers of CD4$^+$ cells from the indicated tissues at 14 dpi. The numbers of CD4$^+$ T cells in uninfected C57BL/6 and CCR2$^{-/-}$ mice were 3.05 $\times$ 10^5 $\pm$ 1.76 $\times$ 10^5 and 9.98 $\times$ 10^5 $\pm$ 4.43 $\times$ 10^5 (liver), 2.95 $\times$ 10^6 $\pm$ 0.50 $\times$ 10^6 and 5.63 $\times$ 10^6 $\pm$ 1.90 $\times$ 10^6 (MLN), and 13.03 $\times$ 10^6 $\pm$ 0.90 $\times$ 10^6 and 17.45 $\times$ 10^6 $\pm$ 1.06 $\times$ 10^6 (spleen), respectively. (C) Percentages of CD4$^+$ T cells that are positive for CD44 were determined by flow cytometry. Means and standard errors are indicated. P values were determined with a Mann-Whitney test, and P values of <0.05 are indicated.

sera from CCR2$^{-/-}$ mice, the signal strength did not increase at 14 dpi (Fig. 5D). When the serum antibody subclass response to secreted Yops was quantified by an enzyme-linked immunosorbent assay (ELISA), the IgM responses were similar in C57BL/6 and CCR2$^{-/-}$ mice at 7 dpi (Fig. 5E). However, levels of IgG1, IgG2b, and IgM increased dramatically from days 7 to 14 postinfection in sera from C57BL/6 mice, but these increases were not observed in sera from CCR2$^{-/-}$ mice (Fig. 5F). Overall, these results indicated a lack of progress and a failure to undergo class switching in the serum antibody response in *Y. pseudotuberculosis*-infected CCR2$^{-/-}$ mice.

The lack of progress beyond an initial IgM response in CCR2$^{-/-}$ mice pointed to decreased help from CD4$^+$ T cells. To examine this possibility, CD4$^+$ T cells in livers, MLNs, and spleens from C57BL/6 and CCR2$^{-/-}$ mice left uninfected or infected for 14 days were enumerated by flow cytometry (representative dot plots are shown in Fig. 6A). In fact, at 14 dpi, CCR2$^{-/-}$ mice carried fewer total CD4$^+$ T cells than did C57BL/6 mice for all tissues analyzed, and the differences were statistically significant for liver and spleen (Fig. 6B). Furthermore, significantly lower percentages of CD4$^+$ T cells in livers and MLNs of CCR2$^{-/-}$ mice expressed the activation marker CD44 (Fig. 6C). These results suggested that CD4$^+$ T cells are less activated in CCR2$^{-/-}$ mice infected with *Y. pseudotuberculosis*. Thus, compared to C57BL/6 mice, CCR2$^{-/-}$ mice have a significant defect in serum antibody responses to *Y. pseudotuberculosis*, in addition to a reduced YopE$_{69-77}$-specific CD8$^+$ T cell response (Fig. 4), suggesting that CCR2$^+$ IMs are critical for multiple arms of adaptive immunity to this pathogen.

DISCUSSION

Previously, using i.v. infection of CCR2$^{-/-}$ mice with a *Y. pseudotuberculosis yopE* GAP mutant, we obtained evidence that CCR2$^+$ IMs are required for host protection from lethal challenge and a dominant YopE$_{69-77}$-specific CD8$^+$ T cell response (31). Here, using oral challenge of CCR2$^{-/-}$ mice with wild-type *Y. pseudotuberculosis*, we extend these results by showing that IMs are also important for a dominant

$YopE_{69-77}$-specific CD8$^+$ T cell response during intestinal infection. Our data also indicate that IMs have a more complex role in immune responses to oral infection with wild-type *Y. pseudotuberculosis*. Specifically, our data suggest that during oral infection, IMs (i) are not required for protection from lethal infection but in fact increase total body weight loss and lymphadenopathy and the persistence of *Y. pseudotuberculosis* in MLNs; (ii) are recruited to the periphery of *Yersinia* pyogranulomas, a process that may be associated with the induction of mesenteric lymphadenopathy and regulation of neutrophil function; (iii) colocalize with CD11c$^+$ cells and $YopE_{69-77}$-specific CD8$^+$ T cells in MLNs, suggesting that these cells can differentiate into DCs to directly prime CD8$^+$ T cells in pyogranulomas; and (iv) are important for a progressive serum antibody response to *Y. pseudotuberculosis*, possibly due to the increased activation of CD4$^+$ T cells, which provide help to B cells.

There are several possible reasons why IMs are important for protection against lethal i.v. infection with a *Y. pseudotuberculosis yopE* GAP mutant but not oral infection with wild-type bacteria. First, the *yopE* GAP mutation, used to attenuate *Y. pseudotuberculosis*, may unintentionally make the bacteria more susceptible to killing by IMs. Specifically, YopE GAP activity blocks ROS production by phagocytes (20), and IMs along with neutrophils are important for ROS production during *Y. pseudotuberculosis* infection (35). Also, YopE GAP activity is important for antiphagocytosis, and its inactivation may render the pathogen toward an intracellular pathway leading to increased killing by IMs. Similarly, in *L. monocytogenes* i.v. infection models, CCR2-dependent IMs and their derivatives, the Tip-DCs, are required for host survival (3). It is possible that for systemic infections resulting from intracellular pathogens, IMs are required for controlling pathogen expansion. Second, the loss of any protective effect of IMs in directly controlling systemic colonization may be counterbalanced by reduced body weight loss, diminished lymphadenopathy and bacterial persistence in MLNs, and a heightened neutrophil response (discussed below) when CCR2$^{-/-}$ mice are orally infected by *Y. pseudotuberculosis*. However, it is important to point out that IMs have been shown to be protective against oral infection by mucosal pathogens, including *Toxoplasma gondii* (36, 37) and *Citrobacter rodentium* (38). This highlights the diverse roles that IMs can play in immune responses to different pathogens.

By 3 dpi, IMs and neutrophils were recruited to MLNs and spleens of CCR2-GFP mice, with IMs being concentrated at the periphery and neutrophils colocalizing with and surrounding the bacteria in *Yersinia* pyogranulomas. This direct contact would allow neutrophils to be injected with Yops from *Y. pseudotuberculosis* (16, 17) but would also put them in a convenient position to phagocytose the bacteria, especially when the effect of inhibition from Yops is not complete. The encircling localization of IMs around neutrophils is consistent with the postulation that IMs regulate neutrophils in *Yersinia* pyogranulomas. The possibility that IMs regulate neutrophils could explain the observation that there was a trend toward or a significant increase in the numbers of neutrophils in tissues such as MLNs and livers of CCR2$^{-/-}$ mice at 3 and 7 dpi compared to control C57BL/6 mice. There are at least two ways in which IMs could regulate neutrophils. One way is to regulate the numbers of neutrophils, and the other is to regulate neutrophil activity. Previously, Davis et al. showed that in *Y. pseudotuberculosis*-infected mouse spleens, neutrophils surround the bacteria, and NO-producing cells are localized in a ring around the neutrophils (14). Our data suggest that CCR2-expressing IMs or IM-derived DCs, which express CD11c, could be an important component of the NO-producing cells observed by Davis et al. NO has been shown to inhibit rolling and adhesion of neutrophils and induces the apoptosis of neutrophils (39). Additionally, Ly6C$^+$ IMs suppress the activity of neutrophils through the production of the lipid mediator prostaglandin E$_2$ (PGE$_2$) in response to a broad range of bacterium-derived ligands, including those recognized by Toll-like receptor 2 (TLR2), TLR4, TLR5, and TLR9 (37). Conceivably, *Y. pseudotuberculosis*, as a bacterial pathogen, is effective at stimulating PGE$_2$ production from IMs. This needs to be tested later. The strategic localiza-

tion of IMs and IM-derived DCs surrounding neutrophils not only allows them to participate in containing *Y. pseudotuberculosis* but also minimizes tissue damage from activated neutrophils and positions them to obtain antigens (discussed below).

The persistent enlargement of the MLNs of *Y. pseudotuberculosis*-infected C57BL/6 mice is consistent with a previous report showing that infection with this strain of *Y. pseudotuberculosis* resulted in chronic lymphadenopathy, which is characterized by 3- to 4-fold tissue enlargement; the formation of central abscesses; the presence of neutrophils, inflammatory monocytes, and foamy macrophages; and significant collagen deposition (12). Lymphadenopathy resulting from acute *Y. pseudotuberculosis* infection can be assessed by the presence of MLNs of >100 mg in a majority (~70%) of the wild-type animals after clearance of *Y. pseudotuberculosis* bacteria from this locale (12). Curiously, of all the CCR2$^{-/-}$ mice that we analyzed after infection, only one carried an MLN that was >100 mg, and this organ was still colonized at 14 dpi (Fig. 1E and H). This result suggested a potential role of CCR2-dependent cells in acute *Yersinia* infection-induced long-term MLN damage. Chronic lymphadenopathy resulting from acute *Y. pseudotuberculosis* infection is associated with lymphatic leakage and microbiota-dependent inflammation in the mesenteric adipose tissue and defects in DC migration to the lymph node (12). It is not yet known whether increased lymphatic leakage causes or directly plays a role in chronic lymphadenopathy, but curiously, NO has been assigned as a key inducer of lymphatic endothelial barrier dysfunction (40). In addition, Fonseca et al. hypothesized that phagocytes driven through lymphatics in response to *Y. pseudotuberculosis* are responsible for lymphatic damage (12). Considering that IMs are most likely major NO producers, and they migrate to MLNs by as early as day 3 postinfection, it is plausible that these cells play a role in lymphatic damage. IM-derived CX3CR1^{int} monocytes migrating to the lamina propria in response to intestinal infection by *Y. pseudotuberculosis* (11) could also contribute to lymphatic damage. IM production of interleukin-1β (IL-1β), which increases the leakiness of distal lymphatic vessels (41), could also play a role in tissue damage, although the serum concentration of this cytokine was not higher in C57BL/6 mice than in CCR2$^{-/-}$ mice infected with *Y. pseudotuberculosis* (data not shown). Finally, we speculate that IM-induced damage to mesenteric lymphatics and adipose tissue is responsible for the increased weight loss of C57BL/6 mice, detected by as early as 4 dpi.

The application of *in situ* tetramer staining (34) allowed us to show that IMs colocalize with YopE$_{69-77}$-specific CD8$^+$ T cells and CD11c$^+$ cells in MLNs of CCR2-GFP mice infected with *Y. pseudotuberculosis*. We were not able to determine if *Y. pseudotuberculosis* colocalizes with YopE$_{69-77}$-specific CD8$^+$ T cells in these experiments, likely because the bacteria were lost during incubation and washing of the unfixed tissue sections. However, based on the presence of Ly6G$^+$ neutrophils in the vicinity of IMs and YopE$_{69-77}$-specific CD8$^+$ T cells, we speculate that IMs injected with YopE are priming naive antigen-specific CD8$^+$ T cells in MLN pyogranulomas. Although MLNs are likely an important organ in which T cell responses are primed during oral *Y. pseudotuberculosis* infection, IMs may function in other tissues to promote adaptive immunity. Bergsbaken and Bevan showed that IM-derived CX3CR1^{int} monocytes enter the lamina propria in response to intestinal *Y. pseudotuberculosis* infection and form immune cell aggregates with CD11c$^+$ cells, adoptively transferred antigen-specific CD8$^+$ T cells, and CD4$^+$ T cells (11). CX3CR1^{int} monocytes appear to function in these clusters to control the differentiation of adoptively transferred CD8$^+$ T cells into a tissue-resident memory phenotype (11, 42). Our data also indicate that IMs are important for optimal CD4$^+$ T cell and B cell responses in MLNs and other organs and the production of serum antibody to *Y. pseudotuberculosis* antigens during oral infection. We suggest that IMs are priming CD4$^+$ T cells in pyogranulomas, which in turn provide help to B cells for antibody production. In this context, IMs were previously implicated in the production of IFN-γ^+ CD4$^+$ T cells in the colon and serum IgG responses to *C. rodentium* during intestinal infection (38). Specifically, Nod2$^{-/-}$ mice, which are deficient in the CCL2-dependent recruitment of IMs to the colon, had reduced numbers of colonic IFN-γ^+

CD4$^+$ T cells and diminished serum IgG responses to *C. rodentium* antigens (38), consistent with the idea that IMs generally may be important for priming adaptive responses to intestinal pathogens.

It may seem surprising that CCR2$^{-/-}$ mice do not show increased susceptibility to primary lethal *Y. pseudotuberculosis* oral infection given their substantial defect in multiple adaptive immune responses at 14 dpi. However, it is important to point out that CD8$^+$ T cell, CD4$^+$ T cell, B cell, and IgM responses were similar between C57BL/6 and CCR2$^{-/-}$ mice at 7 dpi. In addition, NK cell numbers in the MLN, spleen, liver, and blood were similar between C57BL/6 and CCR2$^{-/-}$ mice at 3 and 7 dpi (see Fig. S4 in the supplemental material). Furthermore, reduced adaptive immunity at 14 dpi may be counterbalanced by reduced body weight loss, diminished lymphadenopathy and bacterial persistence in MLNs, and a heightened neutrophil response in CCR2$^{-/-}$ mice. The absence of IMs may remove their direct regulation of neutrophils, leading to a heightened response of these cells. It is also possible that *Y. pseudotuberculosis*-infected CCR2$^{-/-}$ mice would show significantly increased susceptibility to secondary challenge, which would further highlight the positive role that CCR2$^+$ IMs play in promoting adaptive immunity.

MATERIALS AND METHODS

Ethics statement. The use of mice for infection experiments was carried out in accordance with a protocol that adhered to the *Guide for the Care and Use of Laboratory Animals* of the National Institutes of Health (NIH) (43) and was reviewed and approved (approval number 206152) by the Institutional Animal Care and Use Committee at Stony Brook University, which operates under assurance number A3011-01, approved by the NIH Office of Laboratory Animal Welfare.

Mice, infection conditions, and tissue collection and processing. Ccr2$^{-/-}$ mice and CCR2-GFP mice on the C57BL/6 background were provided by Eric Pamer and were bred at Stony Brook University. Age- and sex-matched C57BL/6 mice were purchased from Jackson Laboratory. The *Y. pseudotuberculosis* strain used in this study is serogroup O:1 strain 32777. For oral infection, a bread-feeding model used previously for *L. monocytogenes* (32) was adopted for *Y. pseudotuberculosis*. For this purpose, a bacterial culture of 32777 grown overnight in Luria-Bertani (LB) medium at 28°C was washed once and resuspended in phosphate-buffered saline (PBS) to achieve the desired CFU per milliliter. For each mouse to be infected, a 50-μl volume of the suspension was applied to a single ~0.5-cm³ piece of white bread placed on a thin layer of bedding in the bottom of a cage. Each mouse that had been fasted for 4 h was introduced into a single cage. The entire cage was kept in the dark and checked periodically until the bread was consumed, usually within 1 to 2 h. The mouse was then returned to its original cage. At the indicated times postinfection, or when death was imminent, mice were euthanized by CO$_2$ asphyxiation. When indicated, blood was collected through the tail vein or cardiac puncture and separated into serum after centrifugation in Z-Gel Micro tubes (Sarstedt). Mouse MLNs, spleens, and livers were dissected aseptically and weighed. In addition, where indicated, the left femur was removed to recover the marrow. Spleens and MLNs were homogenized with a 3-ml syringe plunger in 5 ml of fluorescence-activated cell sorter (FACS) buffer (PBS containing 0.2% bovine serum albumin and 2 mM EDTA). Livers were processed with a gentleMACS Dissociator in C tubes (Miltenyi Biotec) according to the manufacturer's instructions. Aliquots from the homogenized tissues were serially diluted in LB medium and plated (100 μl) onto LB agar to determine bacterial colonization by a CFU assay, and the limit of detection was 50 CFU or 1.7 log$_{10}$ CFU.

Immunoblot analysis. Two different growth conditions were used to prepare bacterial lysates. For high-calcium conditions to encourage the synthesis of Yops but to inhibit their secretion into the medium, cultures grown overnight were diluted to an optical density at 600 nm (OD$_{600}$) of 0.1 in LB medium containing 2.5 mM calcium chloride and grown at 37°C with shaking for 2 h. The bacterial cultures were then centrifuged, and the pelleted bacteria were resuspended in PBS. After a second centrifugation, the pelleted bacteria were resuspended in 2× Laemmli sample buffer. This was the bacterial lysate. To prepare secreted Yops, low-calcium conditions, which encourage both the synthesis and secretion of Yops, were used. Cultures grown overnight were diluted to an OD$_{600}$ of 0.1 in LB medium containing 20 mM magnesium chloride and 20 mM sodium oxalate and grown at 28°C for 1 h and then at 37°C for 4 h with shaking. Yop proteins in culture supernatants were precipitated with 10% trichloroacetate, washed once in cold acetone, dried, and resuspended in 1× Laemmli sample buffer.

Bacterial lysates and Yop proteins were resolved by SDS-PAGE, transferred to a nitrocellulose membrane, and analyzed by immunoblotting with mouse serum used as the source of primary antibodies at a dilution of 1:200 (7 dpi) or 1:1,000 (14 dpi or later) and anti-mouse IgG conjugated with IRDye800 (Rockland), as described previously (10).

Flow cytometry. Single-cell suspensions of different organs were prepared as described above (10). Briefly, red blood cells (RBC) were lysed, and viable cells were counted by using trypan blue exclusion with a Vi Cell XR cell viability analyzer (Beckman Coulter). Suspended cells (1 × 10^6 cells) were blocked by using anti-mouse CD16/CD32 (FcγIII/II receptor) clone 2.4G2 (BD Pharmingen) and labeled with allophycocyanin-conjugated MHC class I tetramer K^b YopE$_{69-77}$, which was provided by the NIH Tetramer Core Facility (Emory University, Atlanta, GA), at room temperature for 1 h and fluorophore-conjugated

antibodies on ice for 20 min. The antibodies used were Alexa Fluor 488 or phycoerythrin (PE) anti-mouse CD8α (clone 53-6.7; BD, BioLegend), PE/Cy7 anti-mouse CD3e (clone 145-2C11; Pharmingen), and Brilliant Violet 421 CD44. CD8$^+$ T cells were gated as CD3$^+$ CD8$^+$ events throughout the study. Anti-mouse antibodies used to characterize the leukocytes were Alexa Fluor 488 F4/80 (BM8), peridinin chlorophyll protein (PerCP)/Cy5.5 Ly6C (HK1.4), PE/Cy7 CD11c (N418), Alexa Fluor 700 Ly6G (1A8), Alexa Fluor 647 I-A/I-E (M5/114.15.2), Brilliant Violet 510 CD11b (M1/70), and NK-1.1 Alexa Fluor 488. Antibodies were obtained from BioLegend unless indicated otherwise. Labeled cells were analyzed by using a Cytek DXP 8 color upgrade. Gating on side and forward scatter was used to focus on intact splenocytes, and dead cells were excluded. Data were analyzed with FlowJo software (TreeStar).

Immunofluorescence microscopy. Tetramer staining was carried out with fresh thick sections by using a previously reported protocol (34). Briefly, thick sections of the MLN or spleen were sliced from fresh tissue with a scalpel and incubated with an allophycocyanin (APC)-conjugated YopE$_{69-77}$-specific tetramer together with anti-CD8α antibody (clone 53.6.7) overnight at 4°C in PBS containing 2% fetal bovine serum, 2% normal goat serum, and 30 μg/ml of chloramphenicol (PBS-plus). After washing in PBS, the sections were fixed with 2% paraformaldehyde in PBS and washed and incubated in PBS-plus with rabbit anti-APC and anti-CD8α antibodies overnight at 4°C. When anti-CD11c or Ly6G antibody was used, it was included at this time. Finally, after a wash in PBS, the thick sections were incubated with fluorescence-conjugated species-specific secondary antibodies before imaging.

To analyze the localization of *Yersinia* bacteria in spleen or MLNs, the tissue was fixed with 4% paraformaldehyde in PBS at room temperature for 3 h, washed in PBS, and then sequentially incubated in 15% and then 30% sucrose in PBS at 4°C overnight. The tissue was then snap-frozen in Tissue-Tek OCT compound (Sakura Finetek), and 5-μm sections were prepared and stored at -80°C. The background was first cleared by incubation with a graded series of ethanol through to dimethyl sulfoxide (DMSO) and then back to PBS. The sections were then blocked and incubated with rabbit anti-*Yersinia* antibody, together with either anti-CD11c or Ly6G antibody, followed by 4′,6-diamidino-2-phenylindole (DAPI) staining and fluorescence-conjugated species-specific secondary antibodies, before imaging.

Antibody subclass determination by an ELISA. Antibody subclass determination by an ELISA was carried out as described previously (10). Briefly, the bacterial lysate and secreted Yops, prepared as described above, were used to coat a 96-well MaxiSorp Nunc-Immunoplate at 1 μg/well. Serum samples were collected at the indicated days postinfection and used at dilutions of 1:100 or 1:1,000. Antibody subclasses were assessed with ImmunoPure monoclonal antibody isotyping kit I (Pierce) according to the manufacturer's instructions.

Statistical analysis. Statistical analysis was performed with Prism 5.0 software (GraphPad), and means and standard errors of the means (SEM) were plotted. The tests used are indicated in the figure legends. P values of <0.05 were considered significant.

SUPPLEMENTAL MATERIAL

Supplemental material for this article may be found at https://doi.org/10.1128/IAI .00782-17.

SUPPLEMENTAL FILE 1, PDF file, 0.3 MB.

REFERENCES

1. Lauvau G, Loke P, Hohl TM. 2015. Monocyte-mediated defense against bacteria, fungi, and parasites. Semin Immunol 27:397–409. https://doi .org/10.1016/j.smim.2016.03.014.

2. Xiong H, Pamer EG. 2015. Monocytes and infection: modulator, messenger and effector. Immunobiology 220:210–214. https://doi.org/10.1016/ j.imbio.2014.08.007.

3. Serbina NV, Salazar-Mather TP, Biron CA, Kuziel WA, Pamer EG. 2003. TNF/iNOS-producing dendritic cells mediate innate immune defense against bacterial infection. Immunity 19:59–70. https://doi.org/10.1016/ S1074-7613(03)00171-7.

4. Shi C, Hohl TM, Leiner I, Equinda MJ, Fan X, Pamer EG. 2011. Ly6G$^+$ neutrophils are dispensable for defense against systemic Listeria monocytogenes infection. J Immunol 187:5293–5298. https://doi.org/10.4049/ jimmunol.1101721.

5. Samstein M, Schreiber HA, Leiner IM, Susac B, Glickman MS, Pamer EG.

2013. Essential yet limited role for CCR2(+) inflammatory monocytes during Mycobacterium tuberculosis-specific T cell priming. Elife 2:e01086. https://doi.org/10.7554/eLife.01086.

6. Chung LK, Bliska JB. 2016. Yersinia versus host immunity: how a pathogen evades or triggers a protective response. Curr Opin Microbiol 29: 56–62. https://doi.org/10.1016/j.mib.2015.11.001.

7. Simonet M, Falkow S. 1992. Invasin expression in *Yersinia pseudotuberculosis*. Infect Immun 60:4414–4417.

8. Marra A, Isberg RR. 1997. Invasin-dependent and invasin-independent pathways for translocation of *Yersinia pseudotuberculosis* across the Peyer's patch intestinal epithelium. Infect Immun 65:3412–3421.

9. Logsdon LK, Mecsas J. 2006. The proinflammatory response induced by wild-type Yersinia pseudotuberculosis infection inhibits survival of yop mutants in the gastrointestinal tract and Peyer's patches. Infect Immun 74:1516–1527. https://doi.org/10.1128/IAI.74.3.1516-1527.2006.

10. Zhang Y, Bliska JB. 2010. YopJ-promoted cytotoxicity and systemic colonization are associated with high levels of murine interleukin-18, gamma interferon, and neutrophils in a live vaccine model of Yersinia pseudotuberculosis infection. Infect Immun 78:2329–2341. https://doi.org/10.1128/IAI.00094-10.

11. Bergsbaken T, Bevan MJ. 2015. Proinflammatory microenvironments within the intestine regulate the differentiation of tissue-resident CD8(+) T cells responding to infection. Nat Immunol 16:406–414. https://doi.org/10.1038/ni.3108.

12. Fonseca DM, Hand TW, Han SJ, Gerner MY, Glatman Zaretsky A, Byrd AL, Harrison OJ, Ortiz AM, Quinones M, Trinchieri G, Brenchley JM, Brodsky IE, Germain RN, Randolph GJ, Belkaid Y. 2015. Microbiota-dependent sequelae of acute infection compromise tissue-specific immunity. Cell 163:354–366. https://doi.org/10.1016/j.cell.2015.08.030.

13. Simonet M, Richard S, Berche P. 1990. Electron microscopic evidence for in vivo extracellular localization of Yersinia pseudotuberculosis harboring the pYV plasmid. Infect Immun 58:841–845.

14. Davis KM, Mohammadi S, Isberg RR. 2015. Community behavior and spatial regulation within a bacterial microcolony in deep tissue sites serves to protect against host attack. Cell Host Microbe 17:21–31. https://doi.org/10.1016/j.chom.2014.11.008.

15. Peterson LW, Philip NH, DeLaney A, Wynosky-Dolfi MA, Asklof K, Gray F, Choa R, Bjanes E, Buza EL, Hu B, Dillon CP, Green DR, Berger SB, Gough PJ, Bertin J, Brodsky IE. 30 August 2017. RIPK1-dependent apoptosis bypasses pathogen blockade of innate signaling to promote immune defense. J Exp Med https://doi.org/10.1084/jem.20170347.

16. Durand EA, Maldonado-Arocho FJ, Castillo C, Walsh RL, Mecsas J. 2010. The presence of professional phagocytes dictates the number of host cells targeted for Yop translocation during infection. Cell Microbiol 12:1064–1082. https://doi.org/10.1111/j.1462-5822.2010.01451.x.

17. Maldonado-Arocho FJ, Green C, Fisher ML, Paczosa MK, Mecsas J. 2013. Adhesins and host serum factors drive Yop translocation by yersinia into professional phagocytes during animal infection. PLoS Pathog 9:e1003415. https://doi.org/10.1371/journal.ppat.1003415.

18. Bliska JB, Wang X, Viboud GI, Brodsky IE. 2013. Modulation of innate immune responses by Yersinia type III secretion system translocators and effectors. Cell Microbiol 15:1622–1631. https://doi.org/10.1111/cmi.12164.

19. Black DS, Bliska JB. 2000. The RhoGAP activity of the Yersinia pseudotuberculosis cytotoxin YopE is required for antiphagocytic function and virulence. Mol Microbiol 37:515–527. https://doi.org/10.1046/j.1365-2958.2000.02021.x.

20. Songsungthong W, Higgins MC, Rolan HG, Murphy JL, Mecsas J. 2010. ROS-inhibitory activity of YopE is required for full virulence of Yersinia in mice. Cell Microbiol 12:988–1001. https://doi.org/10.1111/j.1462-5822.2010.01448.x.

21. Westermark L, Fahlgren A, Fallman M. 2014. Yersinia pseudotuberculosis efficiently escapes polymorphonuclear neutrophils during early infection. Infect Immun 82:1181–1191. https://doi.org/10.1128/IAI.01634-13.

22. Rolan HG, Durand EA, Mecsas J. 2013. Identifying Yersinia YopH-targeted signal transduction pathways that impair neutrophil responses during in vivo murine infection. Cell Host Microbe 14:306–317. https://doi.org/10.1016/j.chom.2013.08.013.

23. Rosenheinrich M, Heine W, Schmuhl CM, Pisano F, Dersch P. 2015. Natural killer cells mediate protection against Yersinia pseudotuberculosis in the mesenteric lymph nodes. PLoS One 10:e0136290. https://doi.org/10.1371/journal.pone.0136290.

24. Bergman MA, Loomis WP, Mecsas J, Starnbach MN, Isberg RR. 2009. CD8(+) T cells restrict Yersinia pseudotuberculosis infection: bypass of anti-phagocytosis by targeting antigen-presenting cells. PLoS Pathog 5:e1000573. https://doi.org/10.1371/journal.ppat.1000573.

25. Zhang Y, Mena P, Romanov G, Lin JS, Smiley ST, Bliska JB. 2011. A protective epitope in type III effector YopE is a major CD8 T cell antigen during primary infection with Yersinia pseudotuberculosis. Infect Immun 80:206–214. https://doi.org/10.1128/IAI.05971-11.

26. Russmann H, Gerdemann U, Igwe EI, Panthel K, Heesemann J, Garbom S, Wolf-Watz H, Geginat G. 2003. Attenuated Yersinia pseudotuberculosis carrier vaccine for simultaneous antigen-specific CD4 and CD8 T-cell induction. Infect Immun 71:3463–3472. https://doi.org/10.1128/IAI.71.6.3463-3472.2003.

27. Lin JS, Szaba FM, Kummer LW, Chromy BA, Smiley ST. 2011. Yersinia pestis YopE contains a dominant CD8 T cell epitope that confers protection in a mouse model of pneumonic plague. J Immunol 187:897–904. https://doi.org/10.4049/jimmunol.1100174.

28. Gonzalez-Juarbe N, Shen H, Bergman MA, Orihuela CJ, Dube PH. 2017. YopE specific CD8+ T cells provide protection against systemic and mucosal Yersinia pseudotuberculosis infection. PLoS One 12:e0172314. https://doi.org/10.1371/journal.pone.0172314.

29. Szaba FM, Kummer LW, Duso DK, Koroleva EP, Tumanov AV, Cooper AM, Bliska JB, Smiley ST, Lin JS. 2014. TNFalpha and IFNgamma but not perforin are critical for CD8 T cell-mediated protection against pulmonary Yersinia pestis infection. PLoS Pathog 10:e1004142. https://doi.org/10.1371/journal.ppat.1004142.

30. Zhang Y, Mena P, Romanov G, Bliska JB. 2014. Effector CD8+ T cells are generated in response to an immunodominant epitope in type III effector YopE during primary Yersinia pseudotuberculosis infection. Infect Immun 82:3033–3044. https://doi.org/10.1128/IAI.01687-14.

31. Zhang Y, Tam JW, Mena P, van der Velden AW, Bliska JB. 2015. CCR2+ inflammatory dendritic cells and translocation of antigen by type III secretion are required for the exceptionally large CD8+ T cell response to the protective YopE69-77 epitope during Yersinia infection. PLoS Pathog 11:e1005167. https://doi.org/10.1371/journal.ppat.1005167.

32. Sheridan BS, Pham QM, Lee YT, Cauley LS, Puddington L, Lefrancois L. 2014. Oral infection drives a distinct population of intestinal resident memory CD8(+) T cells with enhanced protective function. Immunity 40:747–757. https://doi.org/10.1016/j.immuni.2014.03.007.

33. Hohl TM, Rivera A, Lipuma L, Gallegos A, Shi C, Mack M, Pamer EG. 2009. Inflammatory monocytes facilitate adaptive CD4 T cell responses during respiratory fungal infection. Cell Host Microbe 6:470–481. https://doi.org/10.1016/j.chom.2009.10.007.

34. Khanna KM, McNamara JT, Lefrancois L. 2007. In situ imaging of the endogenous CD8 T cell response to infection. Science 318:116–120. https://doi.org/10.1126/science.1146291.

35. Green ER, Clark S, Crimmins GT, Mack M, Kumamoto CA, Mecsas J. 2016. Fis is essential for Yersinia pseudotuberculosis virulence and protects against reactive oxygen species produced by phagocytic cells during infection. PLoS Pathog 12:e1005898. https://doi.org/10.1371/journal.ppat.1005898.

36. Dunay IR, Damatta RA, Fux B, Presti R, Greco S, Colonna M, Sibley LD. 2008. Gr1(+) inflammatory monocytes are required for mucosal resistance to the pathogen Toxoplasma gondii. Immunity 29:306–317. https://doi.org/10.1016/j.immuni.2008.05.019.

37. Grainger JR, Wohlfert EA, Fuss IJ, Bouladoux N, Askenase MH, Legrand F, Koo LY, Brenchley JM, Fraser ID, Belkaid Y. 2013. Inflammatory monocytes regulate pathologic responses to commensals during acute gastrointestinal infection. Nat Med 19:713–721. https://doi.org/10.1038/nm.3189.

38. Kim YG, Kamada N, Shaw MH, Warner N, Chen GY, Franchi L, Nunez G. 2011. The Nod2 sensor promotes intestinal pathogen eradication via the chemokine CCL2-dependent recruitment of inflammatory monocytes. Immunity 34:769–780. https://doi.org/10.1016/j.immuni.2011.04.013.

39. Dal Secco D, Paron JA, de Oliveira SH, Ferreira SH, Silva JS, Cunha FDQ. 2003. Neutrophil migration in inflammation: nitric oxide inhibits rolling, adhesion and induces apoptosis. Nitric Oxide 9:153–164. https://doi.org/10.1016/j.niox.2003.11.001.

40. Cromer WE, Zawieja SD, Tharakan B, Childs EW, Newell MK, Zawieja DC. 2014. The effects of inflammatory cytokines on lymphatic endothelial barrier function. Angiogenesis 17:395–406. https://doi.org/10.1007/s10456-013-9393-2.

41. Aldrich MB, Sevick-Muraca EM. 2013. Cytokines are systemic effectors of lymphatic function in acute inflammation. Cytokine 64:362–369. https://doi.org/10.1016/j.cyto.2013.05.015.

42. Bergsbaken T, Bevan MJ, Fink PJ. 2017. Local inflammatory cues regulate differentiation and persistence of CD8+ tissue-resident memory T cells. Cell Rep 19:114–124. https://doi.org/10.1016/j.celrep.2017.03.031.

43. National Research Council. 2011. Guide for the care and use of laboratory animals, 8th ed. National Academies Press, Washington, DC.